

Cite this: *Dalton Trans.*, 2021, **50**, 5184

Investigation of vanadium(III) and vanadium(IV) compounds supported by the linear diaminebis(phenolate) ligands: correlation between structures and magnetic properties†

Zofia Janas,^{*a} Julia Jezierska,^{ID}^a Andrew Ozarowski,^{ID}^{*b} Alina Bieńko,^{ID}^{*a} Tadeusz Lis,^a Adam Jezierski^a and Marta Krawczyk^c

A family of oxidovanadium(IV) compounds containing linear diaminebis(phenolate) (salans) L^{1-5} ligands ($L^1 = [\text{MeNCH}_2\text{CH}_2\text{NMe}(\text{CH}_2-4-\text{CMe}_2\text{CH}_2\text{CMe}_3-\text{C}_6\text{H}_3\text{O})_2]^{2-}$; $L^2 = [\text{MeNCH}_2\text{CH}_2\text{NMe}(\text{CH}_2-4-\text{CH}_3-\text{C}_6\text{H}_3\text{O})_2]^{2-}$; $L^3 = [\text{MeNCH}_2\text{CH}_2\text{NMe}(\text{CH}_2-4-\text{Cl}-\text{C}_6\text{H}_3\text{O})_2]^{2-}$; $L^4 = \{\text{MeNCH}_2\text{CH}_2\text{NMe}[\text{CH}_2-4,6-(\text{CH}_3)_2-\text{C}_6\text{H}_2\text{O}]_2\}^{2-}$; and $L^5 = \{\text{MeNCH}_2\text{CH}_2\text{NMe}[\text{CH}_2-4,6-(\text{Br})_2-\text{C}_6\text{H}_2\text{O}]_2\}^{2-}$) and non-oxidovanadium(III) with $L^{2,4}$ and acac ligands has been prepared and characterized by chemical and physical techniques. Reactions of $[\text{VO}(\text{acac})_2]$ with ligand precursors $\text{H}_2L^{2,4}$ in toluene or hexane afforded vanadium(III) compounds $[\text{V}(\text{L}-\kappa^4\text{ONNO})(\text{acac})]$ (**1**, L^2 ; **2**, L^4), while the use of acetonitrile or ethanol led to the formation of dimeric oxidovanadium(IV) $[\text{VO}]_2(\mu-\text{L}-\kappa^4\text{ONNO})_2$ (**3**, L^1 ; **4**, L^2 ; **5**, L^3) and monomeric $[\text{VO}(\text{L}-\kappa^4\text{ONNO})]$ (**6**, L^4 ; **7**, L^5) compounds. As shown by X-ray crystallography, compounds **1** and **2** are monomeric, in which the chelating ligands afford octahedral *cis*- α geometry at the vanadium center. In the dimeric structures of **3–5**, the six-coordinate vanadium centers are bridged *via* two oxygen atoms of the L^{1-3} ligands while the $L^{4,5}$ ligands generate square pyramidal structures of the monomeric **6** and **7** compounds. HFEPFR studies allowed the determination of the spin Hamiltonian parameters of the $S = 1$ spin state of the monomeric V(III) and dimeric V(IV), and $S = \frac{1}{2}$ in monomeric V(IV) compounds. Magnetic measurements of **3–5** indicated weak ferromagnetic metal–metal exchange interactions. A reaction course for the deoxygenation and reduction of vanadyl–salan compounds is proposed.

Received 18th December 2020,
Accepted 4th March 2021

DOI: 10.1039/d0dt04302h

rsc.li/dalton

The chemistry of vanadium compounds with tetradentate ONNO ligands like Schiff bases (salens) and diaminebis(phenolate) (salans) is of continuous interest to chemists in the context of their relevance to bioinorganic chemistry,¹ molecular magnetism,² catalysis,³ and prospective therapeutic applications.^{3b,4} Among them, those containing salen ligands have mostly been studied. In the last decade, increasing attention has been paid to the salan ligands, salen-reduced variants, which have higher flexibility, stronger nitrogen donors

and greater resistance to hydrolysis than their salen analogues. These features, together with the stabilizing character of the hard phenolate oxygen, allowed the creation of a significant number of oxidovanadium(V) $[\text{VO}(\text{L}-\kappa^4\text{O},\text{N},\text{N},\text{O})(\text{OR})]$ compounds with the general formula $[\text{VO}(\text{salan})(\text{OR})]$ (R = alkyl, aryl). In most cases, the *N*-methylated ligands with different substituents at the *ortho* and *para* positions of the aromatic rings generate octahedral either monomeric or dinuclear V(V) compounds adopting *cis*- α geometry in the solid state, and only one of them has the *cis*- β -type structure.^{3d,4b,5} So far, only a few oxidovanadium(IV) and no V(III) salan compounds have been described.^{5a,d-f} The polynuclear linear chain structures ($\dots\text{V}=\text{O}\dots\text{V}=\text{O}\dots$) have been postulated for $\text{V}^{\text{IV}}\text{O}$ compounds with different salan type ligands, including those derived from chiral diamines, diaminecyclohexane and diphenylethylenediamine, pursuant to low μ_{eff} , $\nu(\text{V}=\text{O})$ values and the EPR spectra.^{5d-f} A synthetic route to the aforementioned compounds involved the reaction of VOCl_2 or VOSO_4 with an appropriate H_2salan in a basic medium. Previously, our research group has succeeded in the preparation of a series of $[\text{V}^{\text{IV}}\text{O}(\text{salan})]$ compounds {salan = $L^1 = [\text{MeNCH}_2\text{CH}_2\text{NMe}(\text{CH}_2-$

^aFaculty of Chemistry, University of Wrocław, 14, F. Joliot-Curie, 50-383 Wrocław, Poland. E-mail: alina.bienko@chem.uni.wroc.pl^bNational High Magnetic Field Laboratory, Florida State University, 1800 E. Paul Dirac Drive, Tallahassee, FL 32310, USA. E-mail: ozarowsk@magnet.fsu.edu^cFaculty of Pharmacy, Wrocław Medical University, 211 Borowska, 50-556 Wrocław, Poland†Electronic supplementary information (ESI) available: Additional crystallographic data for **1**, **2**, and **3–6**; X-band and HF EPR spectra of **3–7** and **2**; additional magnetic data for **3–5** (PDF); and XRD data for **1**, **2** and **3–7** (CIF). CCDC 1997038, 1997039, 1997040, 1997041, 1997042 and 1997043. For ESI and crystallographic data in CIF or other electronic format see DOI: 10.1039/d0dt04302h

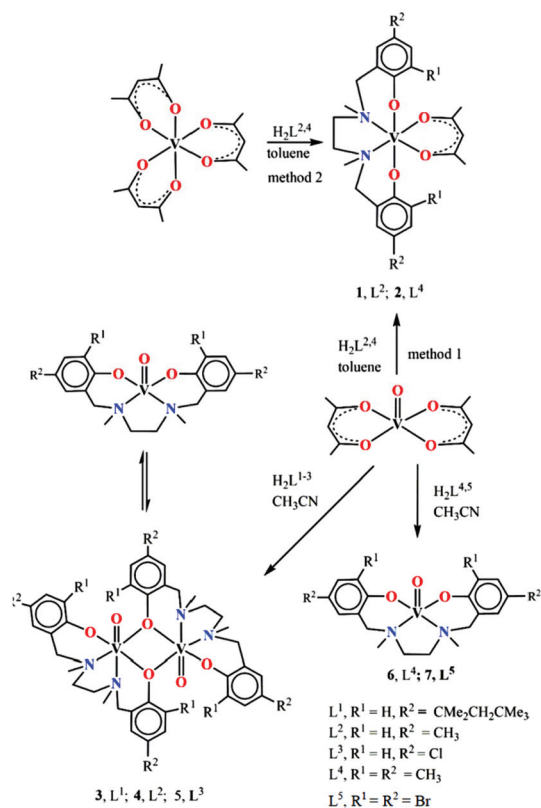
4-CMe₂CH₂CMe₃-C₆H₃O)₂]²⁻; L² = [MeNCH₂CH₂N-Me(CH₂-4-CH₃C₆H₃O)₂]²⁻; and L³ = [MeNCH₂CH₂NMe-(CH₂-4-Cl-C₆H₃O)₂]²⁻ by the reduction of [V^{VO}(salan)(OR)] (R = Me, Et) with *N*-methyl-*N*-phenylhydrazine (NH₂NMePh).^{5a} Previous studies were generally devoted to the potential of salan ligands in the creation of compounds mimicking the active centers of vanadium nitrogenase. Observation of salan-based vanadium (v) compounds oxidizing NH₂NMePh to 2-tetrazene (N₄Me₂Ph₂) has been crucial for a better understanding of the biological formation of hydrazine. It was then demonstrated very clearly by EPR spectra and magnetic studies that all except one V^{VO} compounds, which are the products of [V^{VO}(salan)(OR)] reduction, are formed as insoluble powders containing a mixture of monomeric (*S* = 1/2) and dimeric (*S* = 1) species. Their high stretching frequency $\nu(\text{V}=\text{O})$ at *ca.* 947–960 cm⁻¹ excluded the polynuclear (...V=O...V=O...) structures. The monomeric structure of [VO(salan)]·EtOH {salan = L¹ = [MeNCH₂CH₂NMe(CH₂-4-CMe₂CH₂CMe₃-C₆H₃O)₂]²⁻} was revealed using X-ray studies and at that time, it was the only example of a structurally characterized [V^{VO}(salan)] compound.^{5a}

Therefore, this new work was undertaken to find other synthetic methods of salan-based oxidovanadium(IV) complexes to prepare their crystals in dimeric or monomeric form separately by using various solvents and H₂salans differently substituted in aromatic rings, either *para* in H₂L¹⁻³ or *ortho* and *para* in new H₂L⁴ = {MeNCH₂CH₂NMe[CH₂-4,6-(CH₃)₂-C₆H₂OH]₂]²⁻ and H₂L⁵ = {MeNCH₂CHNMe[CH₂-4,6-(Br)₂-C₆H₂OH]₂]²⁻. The search for selective and efficient synthesis allowed us to discover the decisive influence of solvent polarity on the reaction between V^{VO}(acac)₂ and H₂salan ligands, giving in non-polar solvents the crystals of monomeric V^{III}(salan)(acac) compounds, where salan = L², 1 and L⁴, 2 and in non-polar solvents the V^{IV}O(salan) compounds as dimers with salan = L¹, 3; L², 4 and L³, 5 and as monomers with salan = L⁴, 6 and L⁵, 7 as solids. We also developed a number of other alternative synthetic methods which revealed and confirmed the likely causes of the various products of the above reaction depending on the solvents and salan substitution. We also present here the results of the HF-EPR and magnetic studies of these seven new oxidovanadium(IV) and non-oxidovanadium(III) complexes in correlation with their crystal and molecular structure properties.

Results and discussion

Synthesis of the non-oxidovanadium(III) and oxido-vanadium(IV)-salan compounds

To synthesize oxidovanadium(IV) compounds based on salan ligands, [V^{VO}(acac)₂] was used as the vanadium precursor and various solvents such as toluene, *n*-hexane, acetonitrile and ethanol were used. Unexpectedly, when [V^{VO}(acac)₂] was refluxed with equimolar quantities of H₂L^{2,4} in toluene or *n*-hexane, orange solids of non-oxidovanadium(III) compounds [V^{III}(L^{2,4}-κ⁴ONNO)(acac)] (L², 1; L⁴, 2) were obtained with ~50% yield (method 1 in Scheme 1). The use of [V^{III}(acac)₃] instead



Scheme 1 Synthetic strategy of compounds 1–7.

of [V^{VO}(acac)₂] (method 2 in Scheme 1) improved the yield to 70.0% of 1 and 91.5% of 2. However, refluxing [V^{VO}(acac)₂] with H₂L¹⁻⁵ in acetonitrile or ethanol resulted in the formation of light-violet compounds [(V^{VO})₂(μ-L¹⁻³-κ⁴ONNO)₂] (L¹, 3; L², 4; L³, 5) and [V^{VO}(L^{4,5}-κ⁴ONNO)] (L⁴, 6; L⁵, 7) with 50–70% yield (according to Method A, see the Experimental section). When the above reactions were carried out at room temperature, the formation of desired products was not complete and unreacted [V^{VO}(acac)₂] or [V^{III}(acac)₃] was observed in the post-reaction mixture. To confirm the effect of substituents at the *ortho* position in the salan ligand L on the reduction of vanadium(v) to vanadium(IV) by hydrazine derivatives, compounds 6 and 7 were also prepared *via* the reaction of *in situ* generated [V^{VO}(L⁴-κ⁴ONNO)(OPr)] with NH₂NMe₂ in CH₃CN at room temperature, in a manner similar to that described previously^{5a} (according to Method B, see the Experimental section) with yields of 85.7% of 6; 98.0% of 7. Compounds 1 and 2 are very well soluble in CH₃CN and toluene, and insoluble in *n*-hexane. They are air- and moisture-sensitive both in solution and in the solid state and have to be stored under an inert atmosphere. In contrast, compounds 3–5 are stable in air for several days but their solubility in organic solvents is very limited. The synthetic method presented here was successful in obtaining crystals of 3–7 directly by slow cooling of the post-reaction mixture. It is worth emphasizing that a previously described preparation of compounds 3–5 *via* the reduction of appropriate vanadate precursors by NH₂NMe₂ in

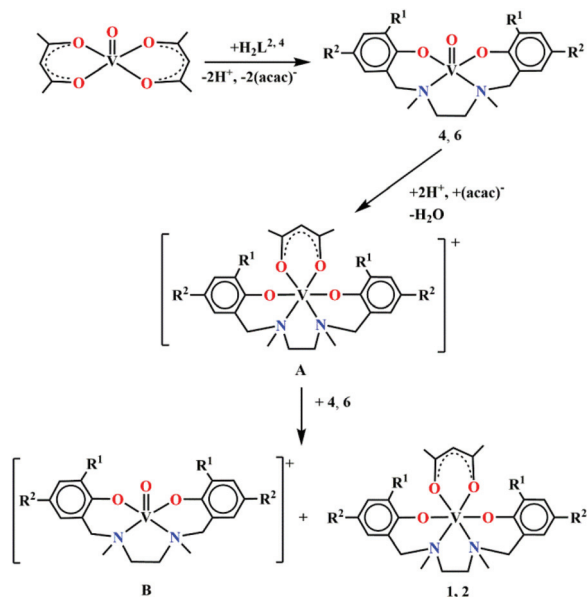
n-hexane resulted in their isolation as completely insoluble powders.^{5a} However, as was shown by EPR spectra and magnetic measurements in ref. 5a and was confirmed in this work, both methods produced 3–5 as a mixture of monomeric and dimeric forms (Scheme 1) and only the crystals of dimers were suitable for crystallographic studies. The monomeric form of 5 was previously isolated from its ethanolic solution and identified by X-ray crystallography.^{5a}

The results of the reactions between $[V^{IV}O(acac)_2]$ and H_2L^{1-5} indicate that the kind of solvent strongly determines the course of the reaction and its product. In polar solvents such as acetonitrile or ethanol, the substitution of the $(acac)^-$ groups in $[VO(acac)_2]$ by the $(L^{1-5})^{2-}$ ligands with elimination of H^+ and $(acac)^-$ occurs to afford vanadyl compounds 3–7 (according to Method A, see the Experimental section). Thus, the question now arises as to why the reactions of $[VO(acac)_2]$ with $H_2L^{2,4}$ produce non-oxido vanadium(III) compounds 1 and 2 in non-polar solvents, toluene or *n*-hexane, respectively. To answer this question, the impact of protons eliminated from $H_2L^{2,4}$ and Hacac during the reaction had to be considered. A probable course of formation of 1 and 2 in toluene or *n*-hexane is proposed in Scheme 2. Compound 4, a mixture of dimeric and monomeric forms, is presented in this scheme as a monomer for simplicity. However, the existence of 4 as a monomer in solution was confirmed by EPR spectroscopy (Fig. S12†).

It is quite likely that in the first stage of the reaction the oxido-vanadium(IV) compounds 4 or 6 are formed by alcoholysis of the V–O(acac) bonds by $H_2L^{2,4}$ and elimination of H^+ and $(acac)^-$ ions. Next, the protonation of the oxido ligand in 4 or 6 by H^+ (from $H_2L^{2,4}$ and Hacac as weak acids) followed by deoxygenation and release of H_2O and $(acac)^-$ most likely

leads to non-oxidovanadium(IV) cationic species A (Scheme 2). Although the intermediate compounds A have not been isolated, their formation was well documented in vanadium chemistry by the reactivity of the V=O moiety with polydentate phenols, including their derivatives functionalized with X-donor atoms (X = N, S, Se, and P).^{6,7,7a,8,9,10} Thus, the octahedral non-oxido-vanadium(IV) compounds such as $[V(L-\kappa^4N, O, O, O)(acac)]$ and $[V(L-\kappa^3X, O, O)_2]$ (X = S and Se) synthesized in the reaction of $[VO(acac)_2]$ with appropriate ligand precursors have been structurally characterized,^{7,8} and other non-oxidovanadium(IV) six-coordinated compounds, $[VCl_2L_4]$ and $[VBr_2L_4]$ with $L_4 = 4O$ and $2N_2O$ donors provided by beta-diketones and Schiff bases, respectively, have been identified and studied in detail by EPR spectroscopy by one of us.^{7a} The final reaction most likely includes the oxidation of a second oxidovanadium(IV) 4 or 6 molecule by A to form an oxidovanadium(V) (B) cation and a neutral non-oxidovanadium(III) $[V(L^{2,4}\kappa^4ONNO)(acac)]$ (1 or 2) complex as the only isolable product. The proposition of such a course is justified by the acid-induced disproportionation of the oxidovanadium(V) salen complexes showing that addition of an equimolar quantity of CF_3SO_3H to solutions of $[V^{IV}O(salen)]$ compounds in anhydrous CH_3CN generates $[V^{V}O(salen)]^+$, $[V^{III}(salen)]^+$ and $[V^{IV}(salen)]^+$ species. Furthermore, the measured formal potentials indicated that $[V^{IV}O(salen)]$ in the presence of an acid is a stronger one-electron oxidant than $[V^{V}O(salen)]^+$.^{3a,11a,b} To verify experimentally the effect of weak organic acids on the reactivity of 4 and 6 depending on the solvent polarity, the reaction of these complexes with $H_2L^{2,4}$ and Hacac at a molar ratio of 1 : 2 : 1, either in toluene (and *n*-hexane) or in CH_3CN (and ethanol), were carried out (see the Experimental section). As a result, the formation of 1 and 2 in toluene or *n*-hexane was confirmed, whereas compounds 4 and 6 in CH_3CN or ethanol remained unchanged. Hence, $H_2L^{2,4}$ together with Hacac provides a sufficiently acidic medium to stimulate the acid-induced disproportionation of 4 and 6 in toluene (or in *n*-hexane) to 1 and 2, respectively. This is consistent with the increase in phenol acidity in non-polar solvents.^{11c,d} Additional acidity is generated by the enol form of Hacac which is dominant in non-polar solvents.^{11d} It should be emphasized that the salen-based non-oxidovanadium(III) compounds are formed in anhydrous CH_3CN but only after acidification by CF_3SO_3H ,^{3a} which is a considerably stronger acid ($pK_a \sim -15$) than Hacac and phenol ligands ($pK_a \sim 9$). It was postulated in our previous report that the lack of substituents at the *ortho* positions of the salen ligands is responsible for the unprecedented reduction of the salen-based oxidovanadium(V) compounds by NH_2NMePh to oxidovanadium(IV) ones and for the oxidation of NH_2NMePh to $PhMeN=N=NMePh$ (2-tetrazene).^{5a}

The aim of our new research was, among others, to find new synthetic routes to the dimeric oxidovanadium(IV) complexes with salen. We expected that *ortho* substituents (Me, Br) in salen $L^{4,5}$ ligands would protect their non-oxidovanadium(V) compounds from reduction by NH_2NMePh because of the formation of the $V_2-\mu-N-NMePh$ intermediate, according to Method B. However it appeared now that the reactions of $[V^{V}O$



Scheme 2 A plausible reaction course for the formation of 1 and 2 in toluene or *n*-hexane.

$[L^{4,5}-\kappa^4ONNO)(OPr)]$ (generated *in situ* with NH_2NMe_2) produced monomeric oxidovanadium(IV) compounds **6** and **7** but with no evidence for the intermediate $V_2-\mu-N-NMePh$ species. Although the *ortho* substituted $L^{4,5}$ ligands did not protect the oxidovanadium(V) center from reduction, they significantly prevented **6** and **7** from dimerization, opposite to **3–5** with the *para*-substituted L^{1-3} ligands which created a mixture of monomeric and dimeric compounds.

Descriptions of structures. Single crystals suitable for X-ray studies of non-oxidovanadium(III) compounds **1** and $2 \cdot 0.25CH_3CN$ and oxidovanadium(IV) compounds **3**, $4 \cdot 2CH_3CN$, $5 \cdot 2CH_3CN$ and **6** were obtained. Their crystal data are given in Table S1.† Selected bond lengths and angles for **1**, $2 \cdot 0.25CH_3CN$ and **3**, $4 \cdot 2CH_3CN$, $5 \cdot 2CH_3CN$, and **6** are given in Tables S2 and S3,† respectively. The perspective views of molecules **2** and **4** are shown in Fig. 1 and 2a, respectively.

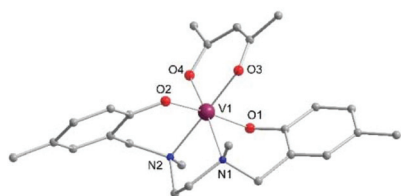


Fig. 1 The molecular structure of **1** with the crystallographic numbering of the donor atoms. Hydrogen atoms have been omitted for clarity.

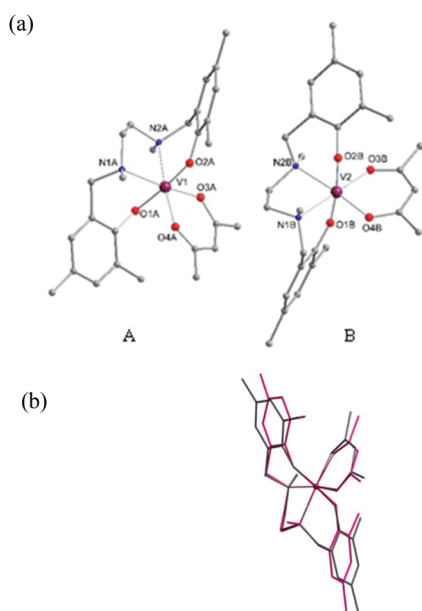


Fig. 2 (a) The molecular structure of two independent molecules found in the crystal of $2 \cdot 0.25CH_3CN$ with the crystallographic numbering of the donor atoms. Hydrogen atoms and CH_3CN molecules of crystallization are omitted for clarity. (b) Overlay of the molecular structures of molecules **A** (marked by red lines) and **B** (marked by gray lines). The molecules were aligned by pairs of atoms: V1 and V2, O1A and O2B, and N1A and N2B.

Compounds **1** and **2** crystallize as monomeric molecules and exhibit *cis-α* geometry with the oxygen donors of the $(acac)^-$ group and the amine nitrogen atoms of the $L^{2,4}$ ligands occupying mutually *cis* coordination sites. The two aryloxy oxygen donors coordinate in a *trans* fashion. This geometry is not surprising since the most structurally characterized salan-metal coordination compounds are *cis-α*.^{1c,3d,4b,5a,c,12a-f,13,14} To our knowledge, compounds **1** and **2** are the first examples of structurally characterized salan-based non-oxidovanadium(III) compounds. In **2**, there are two independent molecules **A** and **B** in the asymmetric unit (Fig. 2a) with slightly different structural parameters as indicated by the overlay of molecules **A** and **B** shown in Fig. 2b. The crystal packing of **2** clearly indicates the influence of the intermolecular interactions such as hydrogen bonding and $C-H \cdots \pi$ contacts on the actual structural parameters of molecules **A** and **B** (Fig. S2 and S3; Tables S4 and S5†). As a consequence, the relevant bond lengths V–O, V–N and angles vary in the range of 0.02–0.04 Å and 5–10°, respectively (see Table S2†). Nevertheless, V–O and V–N bond lengths of the $L^{2,4}$ ligands (av. 1.93 Å and av. 2.20 Å, respectively) as well as the V–O distances of the $(acac)^-$ group (av. 1.99 Å) in **2** and **4** are, within statistical error, in agreement with those observed for $[V(L-\kappa^4O,N,N,O)(acac)]$ $\{L = [Me_2NCH_2CH_2N(CH_2-4,6-Me_2-C_6H_2O)_2]^{2-}\}$, containing the tripod isomer of the linear L^4 ligand.^{15a}

In **1**, the molecules interact *via* $C24-H24C \cdots O1^i$ ($[i] x, 1/2 - y, 1/2 + z$) hydrogen bonds forming chains that stretch along the $[001]$ direction (Fig. S1, Table S6†). Within the chains $C-H \cdots \pi$ interactions between the neighboring molecules of **1** are also observed (Table S7†). In **2**, molecules interact *via* hydrogen bonds of $C23B-H23D \cdots O1A^{ii}$ ($ii = 1/2 - x, -1/2 + y, 1/2 - z$) either within the chains or layers (Fig. S2, Table S4†) and $C-H \cdots \pi$ intermolecular interactions within the chains are observed (Fig. S3, Table S5†).

In the solid state, dimeric molecules **3–5** are very similar, and are exemplified by **4** in Fig. 3 (the molecular structure of **3**, Fig. S4;† of **5**, Fig. S7†). Selected bond distances and angles of **3–5** are presented in Table S3.† As far as we are aware, these are the first dimeric oxidovanadium(IV) salan-based com-

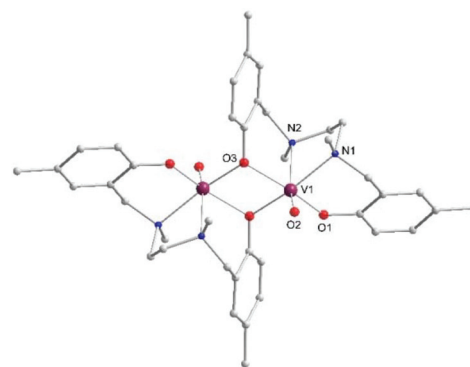


Fig. 3 The centrosymmetric structure of $4 \cdot 2CH_3CN$ with the crystallographic numbering of the donor atoms. Hydrogen atoms and CH_3CN molecules of crystallization have been omitted for clarity.

pounds to be structurally characterized. The central, planar or nearly planar four-membered ring is composed of two vanadium atoms and two bridging oxygen atoms (O3) of the L^{1-3} ligands. The geometry about each vanadium atom is distorted octahedral with three oxygen atoms (the oxido O2 and two aryloxo O1, O3 of the L^{1-3} ligands) and one nitrogen (N1) of the L^{1-3} ligands in the equatorial positions and the second nitrogen (N2) atom of the L^{1-3} ligands and the oxido group occupying the axial sites. As is the case in **1** and **2**, molecules **3–5** exhibit *cis-α* geometry. The V–O_{aryloxo}, V–O_{oxido} and V–N bond lengths in **3–5** are statistically very similar. A significant difference is observed for the V–O1 and V–O3 distances (av. 1.921 and 2.019 Å, respectively) as a consequence of the bridging role of the V–O3 oxygen, whereas the V–N2 bond lengths are significantly longer than V–N1 as a result of a stronger *trans* interaction of the N2 nitrogen with the O2_{oxido} atom.^{15b}

For **3**, **4** and **5** the layered architectures were also considered. Their layers parallel to the (010) plane are shown in Fig. S5, S6 and S8,† respectively. The chains of molecules of **3**, **4** and **5** are held together by C parallel H...π interactions (Tables S8, S9 and S11,† respectively). In the cases of **4** and **5**, molecules of CH₃CN located between the layers are involved in C7–H7A...N1X hydrogen bonds (Tables S10 and S12,† respectively).

In contrast to the dimeric nature of **3–5**, the X-ray study of **6** revealed its mononuclear structure. Its molecular structure is shown in Fig. 4, and selected bond lengths and angles are given in Table S3.†

The coordination environment around the vanadium atom is a distorted square pyramid (trigonality index^{15c} $\tau = 0.17$) with the O₂N₂ set of atoms from the L^4 ligand in the equatorial plane and the oxido group (O2) in an axial position. The O₂N₂ atom set of atoms is significantly distorted from a planar geometry; the vanadium atom is pulled out of the mean equatorial plane by 0.59(2) Å towards the oxido group. The distortion is best illustrated by the variation of the N1–V–O3 and N2–V–O1 angles of 151.13(7) and 140.81(3)°, respectively. Similar structural parameters were observed for the monomeric [VO(L^{1-κ}O, N, N, O)]·EtOH.^{5a} The V–O2_{oxido} distance of 1.602(9) Å is statistically similar to that found in [VO(L^{1-κ}O, N, N, O)] (1.592(1) Å) and is typical of five-coordinate vanadyl species.¹⁶ Both the V–O_{aryloxo} or V–N bond lengths are unequal [V–O1, 1.898(1)

Å; V–O3, 1.922(1) Å and V–N1, 2.200(9) Å; V–N2, 2.167(9) Å] as a consequence of geometric distortion around the vanadium center. Additionally, the V–O_{aryloxo} distances are shorter (~0.03 Å) than those observed for monomeric [VO(μ-L^{1-κ}O, N, N, O)]·EtOH, in which the corresponding distances are probably lengthened by an intermolecular hydrogen-bond interaction with an EtOH molecule.^{5a} The packing diagram of **6** viewed down the [010] direction is shown in Fig. S10.† The crystal structure of **6** exhibits layers parallel to the [010] plane. The adjacent molecules of **6** contact each other *via* C–H...π and π...π interactions (Fig. S11, Tables S13 and S14†).

Compound **6** is the second example of a structurally characterized oxidovanadium(IV) compound bearing the salan ligand.

EPR spectroscopy

The EPR spectra were interpreted in terms of the standard spin Hamiltonian:

$$\hat{H} = \mu_B B \{g\} \hat{S} + D \left\{ \hat{S}_z^2 - \frac{1}{3} S(S+1) \right\} + E(\hat{S}_x^2 - \hat{S}_y^2) + \hat{S}\{A\}\hat{I} \quad (1)$$

The spin Hamiltonian was modified for particular cases: the hyperfine term $\hat{S}\{A\}\hat{I}$ was omitted for the monomeric V(III) compounds **1** and **2**, which exhibited no hyperfine structure. The zero-field splitting terms with D and E are not applicable to the monomeric V(IV) compounds with electronic spin $S = \frac{1}{2}$ and were removed.

The V(III) compounds. Compounds **2** and **4** are silent in X-band EPR, as expected for V(III) in a low symmetry environment.¹⁷ High-field EPR measurements were thus performed for **1** and **2**, the spectra of which are compared in Fig. 5.

It is interesting that compound **2** contains two slightly different molecules as is shown in Fig. 2b and exhibits two distinct EPR spectra (Fig. 5) which is a very rare case. The resolution was sufficient to determine the spin Hamiltonian parameters of each species.

To determine the spin Hamiltonian parameters accurately, a large number of spectra were recorded at various frequencies (like those presented in Fig. 6) and the positions of the canonical transitions, that is those occurring at the molecular X, Y or

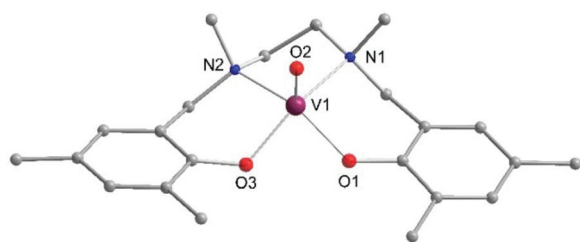


Fig. 4 The molecular structure of **6** with the crystallographic numbering of the donor atoms. Hydrogen atoms have been omitted for clarity.

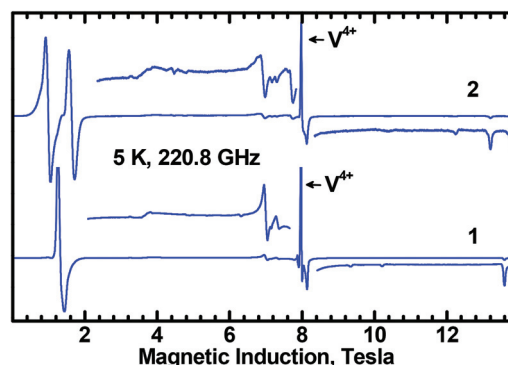


Fig. 5 HF EPR spectra of **1** and **2** recorded under conditions indicated.

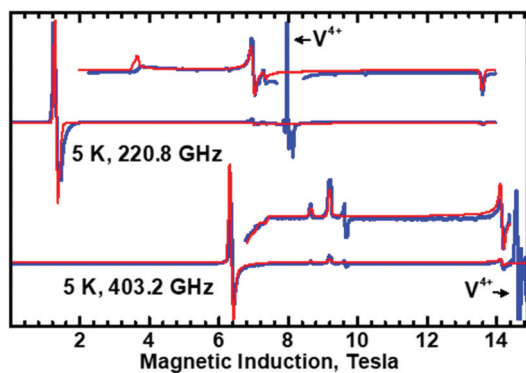


Fig. 6 HFEPR spectra of **1**. Blue: experimental. Red: simulated with parameters in the Fig. 7 caption.

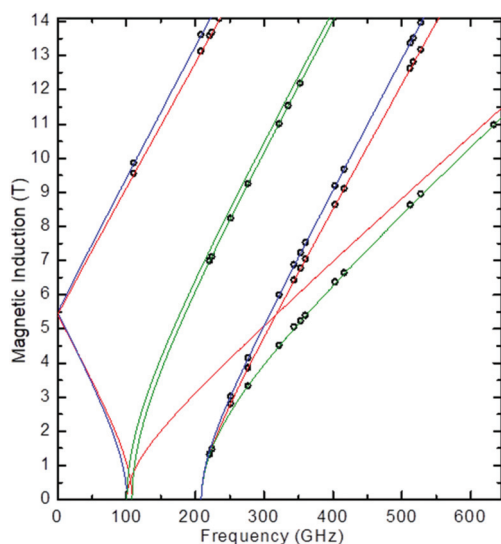


Fig. 7 Frequency dependencies of the resonances observed in **1**. Black circles are the experimental points. The green, blue and red lines were calculated at the molecular orientations *X*, *Y* and *Z*, respectively, using the best-fit parameters $g_x = 1.946(2)$, $g_y = 1.885(1)$, $g_z = 1.978(1)$, $D = 5.288(4) \text{ cm}^{-1}$, and $E = 1.679(3) \text{ cm}^{-1}$.

Z orientations, were fitted (Fig. 7). A similar procedure applied to **2** resulted in the determination of the spin Hamiltonian parameters for two crystallographically independent molecules present in the structure. The parameters are given in the Fig. 8 caption.

An important advantage of the HFEPR is the possibility of determination of the sign of the zero-field splitting parameters D and E . Although the positions of the EPR resonances do not depend on the sign of D or E , the intensity pattern in the low-temperature spectra depends on these signs. This effect relies on the magnitude of the Zeeman energy being comparable to the thermal energy, kT , and not on the magnitude of D . Accordingly, the sign of a very small $|D|$ can also be determined. Compound **1** and both species of **2** have large positive D values in the range $5.1\text{--}5.4 \text{ cm}^{-1}$ and large E values, close to $D/3$.

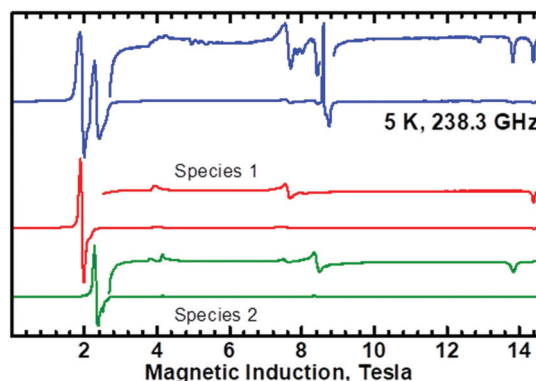


Fig. 8 HF EPR spectra of **2**. Blue: experimental. Red: simulated for species 1 with $g_x = 1.946(6)$, $g_y = 1.889(3)$, $g_z = 1.974(3)$, $D = 5.41(1) \text{ cm}^{-1}$, and $E = 1.69(1) \text{ cm}^{-1}$. Green: simulated for species 2 with $g_x = 1.85(1)$, $g_y = 1.922(3)$, $g_z = 2.005(5)$, $D = 5.115(8) \text{ cm}^{-1}$, and $E = 1.662(4) \text{ cm}^{-1}$.

Dimeric V(IV) compounds. The powder X-band EPR spectra of binuclear compounds **3–5** shown in Fig. 9 show intense central and weaker half field ($\sim 1600 \text{ G}$) lines associated with the allowed ($\Delta M_s = 1$) and forbidden ($\Delta M_s = 2$) resonance transitions, respectively, which occur within the spin triplet state ($S = 1$). The triplet state arises from the exchange coupling of two V^{4+} ions, each bearing one unpaired electron. The V(IV) dimers studied here are not easy to study in HFEPR because of their very small zero-field splitting which at high frequencies becomes comparable to the splitting due to the g anisotropy. Also, the linewidth increases compared to the X-band spectra owing to the g -strain causing disappearance of the hyperfine structure. Nevertheless, the HFEPR spectra of **4** (Fig. 10) allowed us to refine the g values and determine that D and E are positive.

The X-band spectra reveal also a hyperfine splitting of the $\Delta M_s = 1$ and $\Delta M_s = 2$ lines for **4** and **5** and $\Delta M_s = 2$ line for **3** due to coupling of the electron spins with nuclear spins ($I(^{51}\text{V}) = 7/2$) of two vanadium atoms. The observed fifteen-line pattern of hyperfine splitting provides an unambiguous proof

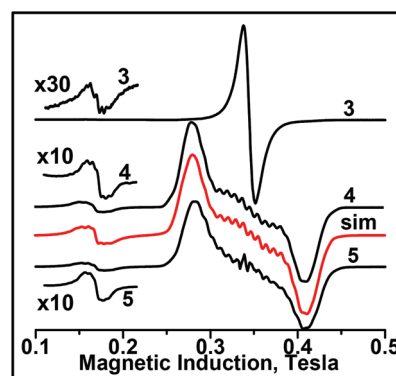


Fig. 9 The X-band EPR spectra of **3–5** at 77 K. The red trace (sim) was simulated with spin Hamiltonian parameters given in the text. The signals due to forbidden $\Delta M_s = 2$ transitions at about 1600 G are also shown at increased amplification.

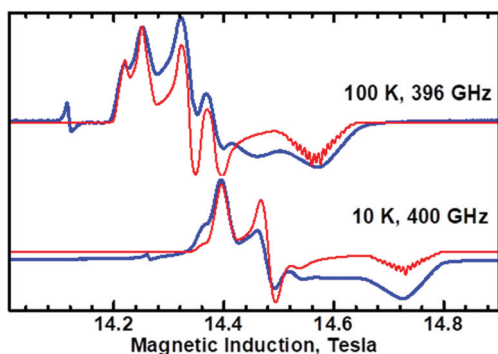


Fig. 10 HF EPR spectra of **4**. The parallel part was simulated with a too small linewidth to show the internal structure of the band. A narrow resonance at 14.1 T (top) and at 14.27 T (bottom) is due to a trace amount of free-radical contamination ($g = 2.0037$).

of the magnetic interaction between two V(IV) centers leading to $S = 1$.

The lack of the lines assigned to $\Delta M_s = 1$ electron transitions in the spectrum of **3**, together with the need for much greater gain to observe the forbidden $\Delta M_s = 2$ line than those for **4** and **5**, indicate a substantial content of monomeric form in **3**, greater than those in **4** and **5**. Simulation of the experimental spin-triplet spectra of **4** and **5**, aided by the HF EPR, allowed the determination of the spin Hamiltonian parameters: $g_x = 1.981$, $g_y = 1.976$, $g_z = 1.942$, $D = 0.007 \text{ cm}^{-1}$, $E = 0.039 \text{ cm}^{-1}$, $A_x = 23 \times 10^{-4} \text{ cm}^{-1}$, $A_y = 27 \times 10^{-4} \text{ cm}^{-1}$, and $A_z = 79 \times 10^{-4} \text{ cm}^{-1}$. The parameters are similar to those obtained previously for the same dimeric oxidovanadium(IV) compounds prepared by us previously by reducing the appropriate oxidovanadium(V)-salan compounds using NH_2NMePh .^{5a} It is especially noteworthy that the spectra of the oxidovanadium(IV) dimers studied here could only be simulated with the E parameters (the measure of rhombicity of ZFS) much larger than D (axial component of ZFS). This relation was observed firstly for the oxidovanadium(IV) dimer with N,N',N'' -trimethyl-1,4,7-triazacyclononane ligands and the bis(μ -hydroxo) bridge implying that the central part of the “allowed” signal corresponds to the parallel orientation.¹⁸ The value of the A_z component ($79 \times 10^{-4} \text{ cm}^{-1}$) of the hyperfine coupling tensor A equals half of that determined for monomeric VO^{2+} compounds, which is expected for binuclear compounds.¹⁹ As normally one finds the D and E parameters obeying the convention $|E| < |D|/3$, a comment will be useful here. The non-conventional set of D and E indicates that the “distinguished” component (that is a component different from the remaining two ones, which are similar to each other) of the zero-field splitting tensor is not parallel to g_z . The g_z component in vanadyl systems is directed roughly towards the axial oxygen atom. The zero-field splitting in a dimeric compound contains a spin-orbit coupling related contribution (also referred to as anisotropic exchange interactions) and a magnetic dipole-dipole contribution. The former one is a major part of the zfs in copper(II) dimeric compounds, in which its distinguished

component D_{zz}^{ex} is parallel to g_z .²⁰ The largest component of the dipole-dipole related zfs contribution is directed along the metal-metal vector. For example, in some copper dimers containing a CuOOCu dibridged unit, similar to the one in our V dimers, an anisotropic exchange contribution, D^{ex} , of about -1 cm^{-1} was observed, while the dipolar contribution was -0.07 cm^{-1} .²¹ The theory of anisotropic exchange is presented in ref. 20. The formulas for the spin-orbit coupling related parts of the zero-field splitting, D^{ex} and E^{ex} , presented in that paper can be adapted to V^{4+} :

$$D^{\text{ex}} = 2 \frac{\xi^2 J_{xy,x^2-y^2}}{\Delta E_{xy,x^2-y^2}} - \frac{1}{4} \frac{\xi^2 J_{xy,yz}}{\Delta E_{xy,yz}} - \frac{1}{4} \frac{\xi^2 J_{xy,xz}}{\Delta E_{xy,xz}} \quad (2)$$

$$E^{\text{ex}} = \frac{1}{4} \frac{\xi^2 J_{xy,yz}}{\Delta E_{xy,yz}} - \frac{1}{4} \frac{\xi^2 J_{xy,xz}}{\Delta E_{xy,xz}} \quad (3)$$

where ξ is the spin-orbit coupling constant (250 cm^{-1} for V^{4+} and 828 cm^{-1} for Cu^{2+}),²² the quantities $J_{xy,xz}$, etc. are exchange integrals in the excited states of a dimer, in which one V^{4+} is in its ground state d_{xy} , while another is in an excited state. $\Delta E_{xy,xz}$, etc. are the ligand-field splittings between the ground state and an excited state of a single ion. Because the terms in the above equations appear in the theory of the g factor, D^{ex} and E^{ex} may also be expressed using the deviation $\Delta g_i = g_i - g_e$ of the g components from the free-electron $g_e = 2.0023$:

$$D^{\text{ex}} = \frac{1}{32} \Delta g_z^2 J_{xy,x^2-y^2} - \frac{1}{16} \Delta g_x^2 J_{xy,yz} - \frac{1}{16} \Delta g_y^2 J_{xy,xz} \quad (4)$$

As the Δg_i values are much smaller in V^{4+} than in Cu^{2+} , it becomes clear that in dimers with similar MOOM bridge arrangements, the zero-field splitting may be dominated by the anisotropic exchange in dinuclear Cu(II) , but not in V(IV) complexes. In the latter ones, the magnetic dipolar contribution becomes larger than the exchange related contribution. The dipole-dipole related part of D may be estimated from

$$D^{\text{dipole}} = -\frac{3g^2\mu_B^2}{2R_{V-V}^3} \quad (5)$$

With an R_{V-V} of 3.25 \AA , one obtains a D^{dipole} of -0.075 cm^{-1} , while $E^{\text{dipole}} = 0$. D^{dipole} and E^{dipole} are expressed in a system of coordinates in which the Z axis is along the V-V direction, but the directions of the axes of the exchange-related zero-field splitting tensor are expected to be parallel to the axes of g . The g_z direction is roughly perpendicular to V-V. Converting the D^{dipole} and E^{dipole} to the coordinates of g (by swapping the Y and Z axes), one obtains $D^{\text{dipole}} = 0.0375 \text{ cm}^{-1}$ and $E^{\text{dipole}} = 0.0375 \text{ cm}^{-1}$. Now, the D^{ex} and E^{ex} can be calculated by subtracting from the experimental D and E values these latter numbers, to obtain $D^{\text{ex}} = -0.030 \text{ cm}^{-1}$ and $E^{\text{ex}} = 0.0015 \text{ cm}^{-1}$. Interestingly, the exchange-related zero-field splitting is close to being axial ($|E^{\text{ex}}|$ small compared to $|D^{\text{ex}}|$). For comparison, in compounds with CuOOCu bridge units, D^{ex} is about 33 times larger.²¹

Frozen solution EPR spectra of dimeric compounds **3–5** in CH_3CN and **4** in CH_2Cl_2 (Fig. S12†) show eight hyperfine lines at both parallel and perpendicular orientations proving the

interaction of $S = 1/2$ with the nucleus spin of one vanadium and hence the formation of mononuclear compounds. Only for **4** in CH_2Cl_2 solution at increased amplification, a weak forbidden line is observed due to the $S = 1$ state. That transition exhibits hyperfine splitting of two vanadium nuclei. The frozen solution spectra of the monomeric compounds **6** and **7** in CH_2Cl_2 are similar to those for the monomers formed from dimeric compounds **3–5** in solutions. The spectra of all these monomeric compounds may be simulated using the same spin Hamiltonian parameters $g_x = g_y = 1.979$, $g_z = 1.947$, $A_x = A_y = 55 \times 10^{-4} \text{ cm}^{-1}$, and $A_z = 163 \times 10^{-4} \text{ cm}^{-1}$, which are typical of oxidovanadium(IV) compounds with the N_2O_2 ligand donor set in the xy plane.²³ This is in agreement with the X-ray structure of **6** and also suggests that the molecular structure of **7**, of which no crystals were obtained, is similar to that of **6**.

Magnetic properties

Dimeric V(IV) compounds. As will be shown below, the metal–metal interactions in compounds **3–5** are surprisingly ferromagnetic in contrast to the strong antiferromagnetic coupling typically reported in the literature for such kinds of complexes.²⁴ Magnetic data were analyzed taking into account the presence of monomeric counterparts of dimers **3–5** (see Scheme 1) in our samples, which was confirmed by EPR spectra. The molar magnetic susceptibility for dimeric oxidovanadium compounds **3–5** has been converted to the χ_{MT} product whose temperature dependence is shown in Fig. 11. The values of χ_{MT} at room temperature which are $1.16 \text{ cm}^3 \text{ mol}^{-1} \text{ K}$ ($3.05\mu_{\text{B}}$) for **3**, $0.94 \text{ cm}^3 \text{ mol}^{-1} \text{ K}$ ($2.96\mu_{\text{B}}$) for **4** and $0.66 \text{ cm}^3 \text{ mol}^{-1} \text{ K}$ ($2.30\mu_{\text{B}}$) for **5** are higher (**3** and **4**) and somewhat lower (**5**) than the expected $0.72 \text{ cm}^3 \text{ mol}^{-1} \text{ K}$ ($\mu_{\text{eff}} = 2.41\mu_{\text{B}}$) for two V(IV) ions without any exchange interactions, with $S = \frac{1}{2}$ and $g_{\text{av}} = 1.97$ taken from EPR. The three dimeric compounds exhibit weak ferromagnetic coupling whose strength increases in the series **3–5–4** (Fig. 11), which can be seen from the shift of the maximum χT towards a higher temperature and an increase in the height of that maximum.

A significant contribution of the temperature independent paramagnetism (TIP) is reflected in the slopes of the χ_{MT} dependencies at higher temperatures. The exchange interaction between two V(IV) ions ($S_{\text{A}} = S_{\text{B}} = \frac{1}{2}$) in **3–5** was described using a model of binuclear units coupled through an aryoxido

bridge. Various additional V...V intermolecular interactions transmitted through the hydrogen bonds are described by the effective zJ' parameter (where z is the number of adjacent binuclear or paramagnetic species around a given binuclear unit). The calculations were based on the Heisenberg–Dirac–Van Vleck Hamiltonian in zero field given using eqn (6)

$$\hat{H} = -J\hat{S}_{\text{A}}\hat{S}_{\text{B}} - zJ'\langle S_z \rangle \hat{S}_z \quad (6)$$

describing the isotropic exchange interaction, ferromagnetic for $J > 0$. The well-known PHI program²⁵ was used which allows for the simultaneous fitting of $\chi T(T)$ and $M(\mu_0 H)$ dependencies. The temperature independent paramagnetism (TIP) and the fraction of monomeric counterparts of dimeric compounds being in equilibrium according to the EPR spectra ($x = 1$ for one uncoupled spin) were also included in the fitting procedure. The best agreement with the experimental magnetic data for **3–5** was obtained with $g = 1.968$, $J = 0.40 \text{ cm}^{-1}$, $zJ' = -0.01 \text{ cm}^{-1}$, $\text{TIP} = 218 \times 10^{-5}$, $x = 0.25$, and $R = \sum[(\chi T)_{\text{calc}}]^2 / \sum[(\chi T)_{\text{exp}}]^2 = 1.84 \times 10^{-5}$ (lines in Fig. 11, left) for **3**; $g = 1.97$, $J = 5.34 \text{ cm}^{-1}$, $zJ' = -0.2 \text{ cm}^{-1}$, $x = 0.33$, $\text{TIP} = 159 \times 10^{-5}$, and $R = 7.37 \times 10^{-6}$ for **4** and with $J = 3.22 \text{ cm}^{-1}$, $zJ' = 0.01 \text{ cm}^{-1}$, $g = 1.96$, $\text{TIP} = 599 \times 10^{-6}$, $x = 0.21$ and $R = 7.04 \times 10^{-7}$ for **5**. The g -values are close to those obtained by simulation of the EPR spectra. The temperature independent paramagnetic term is bigger than that usually obtained.^{2e} Although the origins of the observed phenomenon are unclear, it was verified by repeated measurements. Because of that, TIP was subtracted from the experimental data in Fig. S13† for a better presentation. The PHI program assumes that monomeric contamination is a species with $g = 2$ and $\text{TIP} = 0$. The entire observed TIP is thus ascribed to a dimer, but the contamination here is a monomer of V(IV) whose TIP should be close to half of the dimer TIP. Thus, when applying this method to a situation where the fraction of the monomer is as large as ~ 0.33 (like in **4**), the dimer TIP is obtained too high by a factor of 1.5. It must be emphasized that the synthetic method used in this work produces by its nature a mixture of the dimeric and monomeric species with a considerable fraction of the latter. The variation of magnetization *versus* magnetic field at 2 K (Fig. 11, right) clearly confirms that $S = 1$ is the ground state in dimers **3–5**. Secondly, the magnitude of zJ' demonstrates that the inter-dimer interactions are not negligible.

The explanation of these unexpected ferromagnetic properties does not fit into the theories presented so far. According to Plass's classification,^{2c} compounds **3–5** present an anti-orthogonal configuration in relation to the orientation of the V=O group with respect to the plane defined by the two vanadium centers and two bridging oxygen atoms for which a direct strong antiferromagnetic interaction or superexchange mechanism between the d_{xy} magnetic orbitals could be expected (Fig. S14†). For example, the binuclear octahedral oxidovanadium(IV) compounds with aryoxido, alkoxido and hydroxido bridging ligands show a strong antiferromagnetic feature (with J ranging from -168 to -354 cm^{-1}) (Table S15†).²⁴ Ceccato *et al.* have stated that the J values for

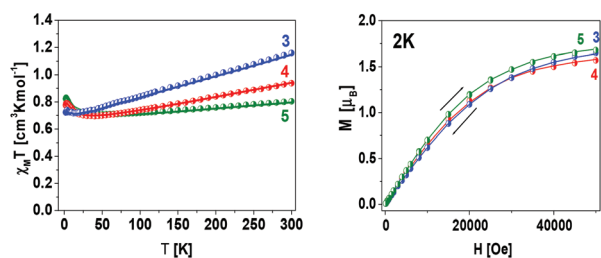


Fig. 11 DC magnetic data for **3–5**. Left – (●) temperature dependence of χ_{MT} . Right – Field dependence of the magnetization per formula unit. The solid lines (on both graphs) are calculated using the HDVV spin Hamiltonian and PHI program.²⁵

those series of compounds are independent of the V–O–V angle, and the V...V and V–μ–O distances, and inferred that the dihedral angle (τ) between the equatorial planes has a decisive impact on the nature and strength of the magnetic interactions (Table S15†).^{24a} The highest antiferromagnetic J values were observed for compounds with the anti- and syn-orthogonal configurations having τ in the range 180–131.1°.^{24a} Although the τ values are 180° or slightly less in compounds 3–5 (Fig. S14†), they exhibit weak ferromagnetic exchange interactions (J is in the range +0.40 to +5.34 cm⁻¹) similar to those for [(VO)₂(HL₂)₂]·MeOH {H₃L = *N*-salicylidene-2-[bis(2-hydroxyethyl)amino ethylamine]}^{2c} having an anti-coplanar configuration, $J = +3.1$ cm⁻¹ and $\tau = 0$. In our opinion, the influence of the value of the V–O–V angle as well as the V...V and V–μ–O distances on the magnitude of magnetic interactions cannot be ignored. The much longer V...V distance and larger V–O–V angle in 3–5 than those in compounds analysed by Ceccato *et al.*^{24a} reduce the overlap between the MOs bearing unpaired electrons resulting in the reduction of the magnitude of magnetic coupling. Moreover, the strength of the intermolecular interaction (zJ') in 4 indicates the importance of secondary exchange pathways which involve the C–H...Cg (π -ring) contacts within the material (Fig. S9†).

Broken symmetry calculations of J in the dimeric compounds. Broken symmetry calculations^{26–28} were performed for compounds 3, 4 and 5 to evaluate the expected magnitude of the exchange integral. In this method, two SCF calculations are performed: in one, the spins on the interacting atoms are assumed parallel and in the second one, they are assumed antiparallel, which is referred to as a broken symmetry state. The J value is subsequently evaluated from the energy difference between the high-spin state and the broken symmetry state,²⁹

$$J = 2(E_{\text{HS}} - E_{\text{BS}}) / [S_{\text{HS}}(S_{\text{HS}} + 1) - S_{\text{BS}}(S_{\text{BS}} + 1)]$$

The ORCA software package³⁰ was employed. The B3LYP/G functional was used with TZVPP functions for all atoms.^{31–33} The calculations produced ferromagnetic J values of 21 cm⁻¹, 35 cm⁻¹ and 29 cm⁻¹ for 5, 6 and 7, respectively. In the experience of some of us, we observed that the method tends to produce overestimated (by some 50%) but reasonable J values. The decidedly too large values calculated by ORCA in our three cases are thus disappointing. For comparison, we performed a similar DFT calculation for a strongly antiferromagnetically coupled bis(μ -hydroxo)bis[oxo(1,4,7-triazacyclononane vanadium(IV))] dibromide, for which $J = -354$ cm⁻¹ was determined from the magnetic data obtained by Wieghardt *et al.*^{24d} The calculation produced $J = -540$ cm⁻¹. The striking difference between our dimers and the triazacyclononane (TCNA) compound was thus reproduced. It is known that the overlap of the magnetic orbitals containing the unpaired electrons of two interacting ions gives rise to the antiferromagnetic coupling. For 3, 4 and 5 the overlap integrals of the magnetic orbitals (calculated by the broken symmetry procedure) were 0.027, 0.019 and 0.022, respectively, while it was equal to 0.13 for the TCNA compound. The trend of the J values is parallel

to the trend of the overlap integrals, with the ferromagnetism increasing (or antiferromagnetism decreasing) when the overlap is reduced. The orbital overlap in 4 and in the TCNA compound is shown in Fig. 12. The dramatic dependence of J on the orbital overlap suggests that the magnitude and sign of J depend on how well the d_{xy} orbitals of two V⁴⁺ ions are aimed at each other, and the empirical rules described above may not be perfect in predicting this, while the DFT software is successful, at least qualitatively. The very steep correlation between the orbital overlap and J may also be a reason for the unsatisfactory numerical values of the calculated J values.

Monomeric V(III) and V(IV) compounds

Since the spin Hamiltonian parameters g , D and E are already known from EPR spectra (Fig. S15†), the magnetic susceptibility measurements for monomeric non-oxidovanadium(III) 1, 2 and oxidovanadium(IV) 6, 7 appear to be superfluous, particularly because the bulk magnetic susceptibility is weakly sensitive to D and E . Nevertheless, this technique can provide information on intermolecular interactions and spin states (Fig. S16–S18†).

At room temperature, the effective magnetic moments are 2.58 μ_{B} and 3.02 μ_{B} for 1 and 2, respectively, a little different from that expected for $S = 1$ (V³⁺), nevertheless they are consistent with vanadium(III) d² species. A similar effective magnetic moment to 2 was observed for [V(L)(acac)] {L = [Me₂NCH₂CH₂N(CH₂-4,6-Me₂-C₆H₂O)₂]²⁻} (2.91 μ_{B} , 295 K).¹⁵ In the case of monomeric oxidovanadium(IV) compounds 6 and 7 the effective magnetic moments at room temperature are 1.99 μ_{B} and 1.84 μ_{B} , respectively, which are close to that expected for $S = \frac{1}{2}$ spin of vanadium(IV) d¹ species. The inter-

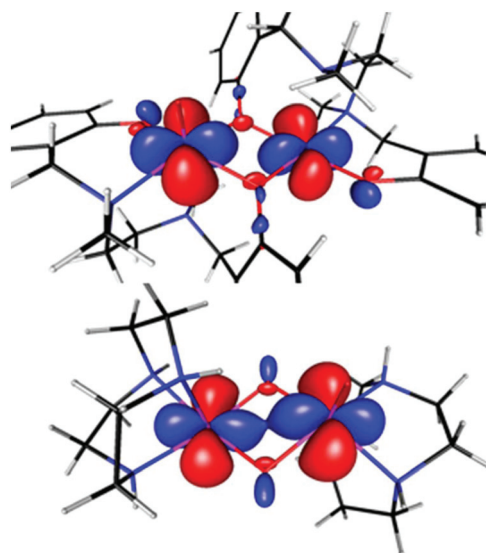


Fig. 12 Overlap of the magnetic xy orbitals in bis(μ -hydroxo)bis[oxo(1,4,7-triazacyclononane vanadium(IV))] dibromide (bottom) and in 4 (with some outer parts cut off for clarity). The symmetric orbitals (thus belonging to $S = 0$) are plotted at an isosurface value of 0.04. The Z axis is perpendicular to the VOOV bridge plane.

molecular interactions in all monomeric complexes were calculated according to the procedure described in the ESI.† The resulting zJ' values, -0.14 cm^{-1} for **2**, -0.01 cm^{-1} for **6**, and -0.08 cm^{-1} for **7**, indicate that a weak exchange interaction between the nearest vanadium atoms in the crystal lattices can exist but in the cases of **1** and **2** the zero-field splitting effect of the V^{3+} ions ($D = 5.29\text{ cm}^{-1}$ (**1**) and $D = 5.26\text{ cm}^{-1}$ (**2**) according to our HFEPR studies) is predominant, which affects the decrease of $\chi_M T$ in the low temperature range.

Calculations of D in **5.** In recent years, density functional theory (DFT) and *ab initio* methods have been applied to gain insight into the nature of zero-field splitting.^{34,35} We have attempted to calculate the spin-orbit coupling contribution to D and E in our compound **5** using the state-averaged complete active space self-consistent field (CASSCF)^{34,35} approach, with 2 electrons in 5 orbitals. 10 triplet states have been taken into account. Similar to our broken symmetry calculations above, the B3LYP functional was used with def-2 TZVPP functions³⁶ for all atoms. The calculations showed that $D = -10.0\text{ cm}^{-1}$ and $E/D = 0.19$. The result is thus disappointing, as the experimental data are $D = +5.29\text{ cm}^{-1}$ and $E/D = 0.31$. The sign of D is difficult to determine theoretically when the E/D ratio is high. With the “maximum rhombicity”, that is $E/D = 1/3$, the diagonalized traceless zero-field splitting tensor has three components, $D_{xx} = 0$, $D_{yy} = -(2/3)D$ and $D_{zz} = (2/3)D$, and powder EPR spectra simulated with either negative or positive D will be identical, even at the lowest temperatures. With $|E/D|$ slightly smaller than $1/3$, the sign of D depends on a small deviation of D_{xx} towards either D_{yy} or D_{zz} , the calculation of which may well be beyond the accuracy of theoretical methods. The wrong sign of D obtained from CASSCF is thus not necessarily worrisome, while the absolute magnitude of D still is. Large differences between the theoretically calculated^{37a} and experimental^{37b} D parameters for $V(\text{III})$ complexes were also obtained by others. It should be emphasized that the sign of D can be determined experimentally by HFEPR even at E/D ratios close (but not equal) to $1/3$, provided that the Y and Z transitions are spectrally resolved, as is the case here.

Conclusions

In conclusion, vanadium compounds containing salan ligands with either *para* or *para* and *ortho* substituents on the aromatic rings are presented. Two synthetic methodologies were used to obtain oxidovanadium(IV) compounds. The first is a high-yield reduction of appropriate oxidovanadium(V) precursors by NH_2Me_2 in CH_3CN to obtain **6** and **7**. The second route involving reactions of $[\text{VO}(\text{acac})_2]$ with H_2L^{1-5} in CH_3CN or EtOH is admittedly less efficient but capable of obtaining compounds **3–6** in crystalline form. The use of toluene or *n*-hexane instead of CH_3CN for the latter reactions resulted in the formation of non-oxidovanadium(III) compounds **1** and **2**. It has been proved that H^+ eliminated from $\text{H}_2\text{L}^{2,4}$ generates a sufficiently acidic medium in toluene or *n*-hexane to stimulate the acid-induced disproportionation of **4** and **6** and is responsible for

their reduction to **1** and **2**. Compounds **1**, **2** and **3–5** are the first examples of structurally characterized non-oxidovanadium(III) and dimeric oxidovanadium(IV) salan-based species. The structures of the oxidovanadium(IV) compounds were found to be controlled by the substituent position in aromatic rings at the salan ligands as well as by the solvent. The $\text{L}^{4,5}$ ligands substituted at *ortho* positions (besides *para*) generate monomeric oxidovanadium(IV) (**6** and **7**) compounds, whereas the L^{1-3} ligands substituted at *para* positions favor the formation of a mixture of dimeric and monomeric forms (**3–5**) in the solid state, while in solution the monomeric molecules dominate. Furthermore, the *para* substitution of $\text{L}^{4,5}$ ligands does not protect the vanadium(V) in oxidovanadium(V) compounds from reduction by substituted hydrazine, but significantly prevent the dimerization of monomeric $[\text{VO}(\text{L}^{4,5}\text{-}\kappa^4\text{ONNO})]$ species.

The comprehensive analysis of HFEPR spectra proved that the metal centers in **1** and **2** are the $V(\text{III})$ ($S = 1$) ions in low symmetry coordination as indicated by the characteristic zero-field splitting parameters D and E in the ranges of $5.1\text{--}5.4\text{ cm}^{-1}$ and $1.66\text{--}1.69\text{ cm}^{-1}$, respectively. The presence of two slightly different molecules in the crystal structure of **2** resulted in the rare observation of two distinct HFEPR spectra with slightly differing parameters. The X-band and HFEPR spectra confirmed the dimeric structure of $V(\text{IV})$ compounds **3–5**, the spectra of which are characteristic of $S = 1$ with hyperfine splitting due to two $V(\text{IV})$ nuclei and an unusual $|E| > |D|/3$ relation, which could be explained. Magnetic measurements have shown that compounds **3–5** are rare examples of dimeric forms of oxidovanadium(IV) with unusual, weak ferromagnetic interactions in contrast to the strong antiferromagnetic interactions expected for the anti-orthogonal configuration. These results have been confirmed also by the theoretical calculations.

Experimental

Materials and methods

Caution! 1,1-Dimethylhydrazine is an acutely toxic chemical. It can cause burns to the skin and eyes and is highly irritating to the mucous membranes. All operations should be conducted in a well-ventilated fume hood and behind a safety shield.

All operations were carried out under a dry dinitrogen atmosphere, using standard Schlenk techniques. All solvents were distilled under dinitrogen using appropriate drying agents. Reagents were purchased from Aldrich Chemical Co. and used without further purification unless stated otherwise. Ligand precursors H_2L^{1-5} were conducted through procedures previously described.^{4b,5a,13,38,39}

Synthesis

$[\text{V}^{\text{III}}(\text{L}2,4\text{-}\kappa^4\text{O,N,N,O})(\text{acac})]$ (**1**, **2**). *Method 1.* To a solution of ligand precursors $\text{H}_2\text{L}^{2,4}$ in toluene or *n*-hexane $[\text{V}^{\text{IV}}\text{O}(\text{acac})_2]$ was added (1 : 1 ratio) and the blue-green mixture obtained was refluxed for about 15 h (toluene) or 3 days (*n*-hexane) resulting in a brown solution or a light-brown solid, respect-

ively. In the case of the toluene post-reaction mixture, all volatiles were removed *in vacuo* to dryness to yield dark-orange products which were washed with *n*-hexane and dried under vacuum. Diffraction-quality bright-orange crystals of **1** and 2·0.25CH₃CN were obtained by recrystallizing from toluene and acetonitrile, respectively, at room temperature. Crystals of **1** and **2** were characterized as follows:

1: Yield: 53%. Calcd for C₂₅H₃₃N₂O₄V: C 63.00, H 6.98, N 5.88. Found: C 62.87, H 6.89, N 5.81%. $\mu_{\text{eff}} = 2.58\mu_{\text{B}}$ (300 K).

2·0.25CH₃CN: Yield: 49.5%. Calcd for C₂₇H₃₇N₂O₄V·0.25CH₃CN (C_{27.5}H_{37.75}N_{2.25}O₄V): C 64.26, H 7.40, N 5.55. Found: C 64.19, H 7.36, N 5.51%. $\mu_{\text{eff}} = 3.02\mu_{\text{B}}$ (300 K).

Method 2. The synthesis of compounds **1** and **2** was carried out in toluene according to method 1 using [V^{III}(acac)₃] in place of [VO^I(acac)₂]. Recrystallization from toluene and acetonitrile gave bright-orange crystals of **1** and 2·0.25CH₃CN, respectively. The analysis and crystal data proved to be identical to those obtained by method 1.

1: Yield: 70.0%. Calcd for C₂₅H₃₃N₂O₄V: C 63.00, H 6.98, N 5.88. Found: C 62.94, H 6.96, N 5.84%. Unit cell parameters: $a = 12.011(3)$ Å, $b = 14.728(3)$ Å, and $c = 13.307(3)$ Å; $\beta = 97.28(2)^\circ$.

2·0.25CH₃CN: Yields: 91.5%. Calcd for C₂₇H₃₇N₂O₄V·0.25CH₃CN (C_{27.5}H_{37.75}N_{2.25}O₄V): C 64.26, H 7.40, N 5.55. Found: C 64.25, H 7.41, N 5.56%. Unit cell parameters: $a = 13.237(3)$ Å, $b = 15.650(4)$ Å, and $c = 25.711(7)$ Å; $\beta = 99.83(3)^\circ$.

[(V^{IV}O)₂(μ -L¹⁻³- κ^4 O,N,N,O)] (**L**¹, **3**; **L**², **4**; **L**³, **5**) and [V^{IV}O(μ -L^{4,5}- κ^4 O,N,N,O)] (**L**⁴, **6**; **L**⁵, **7**). **Method A.** A mixture of [VO(acac)₂] and H₂L¹⁻⁵ (1:1 ratio) in acetonitrile or ethanol (50 cm³) was refluxed, whereupon the solution turned from blue-green to dark violet over the course of at least 24 h. Then the post-reaction mixture was left for slow cooling to room temperature. After few days, bright-violet crystals of **3**, 4·2CH₃CN, 5·2CH₃CN and **6** suitable for X-ray studies were formed. Compound **7** precipitated as a dark violet solid in hot acetonitrile. The products were filtered off, washed with cold CH₃CN, and dried *in vacuo*. In the case of reactions in ethanol, the resulting dark violet solids were washed with hot acetonitrile to give bright violet microcrystalline products. Compounds **3**–**7** were characterized as follows:

3: Yield: 48.5%. Calcd for C₆₈H₁₀₈N₄O₆V₂: C 69.24, H 9.23, N 4.75. Found: C 69.12, H 9.18, N 4.68%. IR (mineral oil mulls, cm⁻¹): ν (V=O), 960 (s, shr). $\mu_{\text{eff}} = 3.05\mu_{\text{B}}$ (300 K).

4·2CH₃CN: Yield: 51.0%. Calcd for C₄₄H₅₈N₆O₆V₂: C 60.82, H 6.73, N 9.61. Found: C 60.94, H 6.60, N 9.62%. IR (mineral oil mulls, cm⁻¹): ν (V=O), 947 (s, shr). $\mu_{\text{eff}} = 2.96\mu_{\text{B}}$ (300 K).

5·2CH₃CN: Yield: 49.0%. Calcd for C₄₀H₄₆Cl₄N₆O₆V₂: C 50.54, H 4.88, N 8.84. Found: C 50.18, H 4.83, N 8.89%. IR (mineral oil mulls, cm⁻¹): ν (V=O), 959 (s, shr). $\mu_{\text{eff}} = 2.30\mu_{\text{B}}$ (290 K).

6: Yield: 53.0%. Calcd for C₂₂H₃₀N₂O₃V: C 62.70, H 7.18, N 6.65. Found: C 62.63, H 7.17, N 6.58%. IR (mineral oil mulls, cm⁻¹): ν (V=O), 963 (s). $\mu_{\text{eff}} = 1.99\mu_{\text{B}}$ (300 K).

7: Yield: 69.3%. Calcd for C₁₈H₁₈Br₄N₂O₃V: 31.75, H 2.66, N 4.11. Found: C 31.74, H 2.71, N 4.12%. IR (mineral oil mulls, cm⁻¹): ν (V=O), 987 (s). $\mu_{\text{eff}} = 1.84\mu_{\text{B}}$ (300 K).

[V^{IV}O(μ -L^{4,5}- κ^4 O,N,N,O)] (**L**⁴, **6**; **L**⁵, **7**). **Method B.** Compounds **6** and **7** were synthesized by applying slight modifications to the procedure described previously by us for **3**–**5**.^{5a} To *in situ* generated [V^{VO}(L- κ^4 O,N,N,O)(OPr)] (equimolar amounts of [VO(OPr)₃] and H₂L=H₂L^{4,5} in CH₃CN stirred for 2 h), NH₂NMe₂ (1 equiv. of V) was added. The mixture was stirred for 24 hours at room temperature yielding dark-violet solids of **6** and **7**. They were filtered off, washed with CH₃CN and dried under vacuum.

6: Yield: 85.7%. Calcd for C₂₂H₃₀N₂O₃V: C 62.70, H 7.18, N 6.65. Found: C 62.72, H 7.19, N 6.64%. IR (mineral oil mulls, cm⁻¹): ν (V=O) 964 (s). The diluted bright-violet filtrate left at room temperature for few weeks produced few dark-violet crystals, which was confirmed by X-ray analysis to be identical to **6** obtained by method 1.

7: Yield: 98.0%. Calcd for C₁₈H₁₈Br₄N₂O₃V: 31.75, H 2.66, 4.11. Found: C 31.85, H 2.68, N 4.10%. IR (mineral oil mulls, cm⁻¹): ν (V=O), 988 (s).

Reactions of 4 and 6 with H₂L^{2,4} and Hacac. (a) Compounds **4** and **6** (0.5 mmol), Hacac (1.0 mmol), and H₂L^{2,4} (1.0 mmol) in toluene or *n*-hexane (10 cm³) were heated under reflux for 24 h. The resulting brown solutions were evaporated to dryness, and the residues recrystallized from toluene or CH₃CN, and identified as **1** and **2**, respectively, by elemental analysis and unit cell parameters.

1: Yields: 49.5%. Calcd for C₂₅H₃₃N₂O₄V: C 63.00, H 6.98, N 5.88. Found: C 63.09, H 7.01, N 5.89%. Unit cell parameters: $a = 12.011(3)$ Å, $b = 14.728(3)$ Å, and $c = 13.307(3)$ Å; $\beta = 97.28(2)^\circ$.

2·0.25CH₃CN: Yields: 40.0%. Calcd for C₂₇H₃₇N₂O₄V·0.25CH₃CN (C_{27.5}H_{37.75}N_{2.25}O₄V): C 64.26, H 7.40, N 5.55. Found: C 64.31, H 7.53, N 5.51%. Unit cell parameters: $a = 13.237(3)$ Å, $b = 15.650(4)$ Å, and $c = 25.711(7)$ Å; $\beta = 99.83(3)^\circ$.

(b) The reactions of **4** or **6** with Hacac and H₂L^{2,4} were carried out according to procedure (a) using acetonitrile or ethanol. Neither a color change nor the formation of new products was observed after refluxing the reaction mixture for two days.

General instrumentation

Infrared spectra were recorded on a PerkinElmer 180 spectrophotometer in Nujol mulls. Microanalyses were conducted on a Vario EL III CHNS elemental analyzer (in-house).

The X-band electron paramagnetic resonance (EPR) spectra of the oxidovanadium(IV) complexes were recorded using a Bruker ELEXYS E 500 spectrometer equipped with an NMR teslameter and X-band frequency counter. High-frequency EPR spectra were recorded on a 17 T transmission instrument of the EMR facility. The instrument is equipped with a superconducting magnet (Oxford Instruments) capable of reaching a field of 17 T. Microwave frequencies in the range 52–630 GHz were generated using a phase-locked Virginia Diodes source, producing a base frequency of 8–20 GHz, which was multiplied by a cascade of frequency multipliers. The instrument is a transmission-type device and uses no resonance cavity.³⁹ Both

the X-band and high-field EPR spectra were simulated using computer programs written by one of us.⁴⁰

The magnetic susceptibility measurements were made using a Quantum Design MPMS-3 SQUID magnetometer in the temperature range 1.8–300 K in a magnetic field of 0.5 T. The susceptibilities of **1–6** have been corrected for the diamagnetic contribution using Pascal's constants.⁴¹

X-ray diffraction data for **1**, **4** and **5** were obtained using an Xcalibur PX diffractometer with a CCD Ruby camera and for **2**, **3** and **6** using a KM4 diffractometer with a CCD graphite camera and Mo K α radiation ($\lambda = 0.71073 \text{ \AA}$) at 100 K.⁴¹ The experimental details and crystal data are given in Table S1 in the ESI.† The structures were solved by direct methods and refined by full-matrix least-squares techniques on all F^2 data using the SHELXTL software.⁴² All non-hydrogen atoms were refined with anisotropic thermal parameters. All hydrogen atoms were placed in geometrically calculated positions and refined using a riding model with U_{iso} set at $1.2U_{\text{eq}}(\text{C})$ for aromatic and methylene H atoms, and at $1.5U_{\text{eq}}(\text{C})$ for methyl H atoms. In **3**, the C atoms of methyl groups in the $\text{C}(\text{CH}_3)_2\text{CH}_2\text{C}(\text{CH}_3)_3$ substituent are disordered and they were modeled and refined in two positions with site occupancy factors (s.o.f.) of 0.907 and 0.093.

CCDC reference numbers: 1997038 for **1**, 1997039 for **2**·0.25CH₃CN, 1997040 for **3**, 1997041 for **4**·2CH₃CN, 1997042 for **5**·2CH₃CN and 1997043 for **6**·2CH₃CN.†

Conflicts of interest

There are no conflicts to declare.

Acknowledgements

The authors thank the National Scientific Centre (Narodowe Centrum Nauki) for the financial support of this work. (Poland, grant no. 2012/05/N/ST5/00697). The National High Magnetic Field Laboratory is supported by the National Science Foundation through the Cooperative Agreement DMR-1644779 and the State of Florida.

Notes and references

- (a) D. C. Crans, J. J. Smee, E. Gaidamauskas and L. Yang, *Chem. Rev.*, 2004, **104**, 849–902; (b) B. A. MacKay and M. D. Fryzuk, *Chem. Rev.*, 2004, **104**, 385–402; (c) D. Rehder, *Bioinorganic Vanadium Chemistry*, John Wiley & Sons, Ltd., New York, 2008.
- (a) O. Kahn, *Molecular Magnetism*, VCH, New York, 1993; (b) D. Christou, D. Gatteschi, D. N. Hendrickson and R. Sessoli, *MRS Bull.*, 2000, **25**, 66–71; (c) W. Plass, *Angew. Chem., Int. Ed. Engl.*, 1996, **35**, 627–631; (d) M. Tsuchimoto and N. Yoshioka, *Chem. Phys. Lett.*, 1998, **297**, 115–120; (e) W. Plass, *Z. Anorg. Allg. Chem.*, 1997, **623**, 1290–1298.
- (a) E. Tsuchida and K. Oyaizu, *Coord. Chem. Rev.*, 2003, **237**, 213–228; (b) J. C. Pessoa and I. Correia, *Coord. Chem. Rev.*, 2019, **388**, 227–247; (c) Y. Chen, S. Yekta and A. K. Yudin, *Chem. Rev.*, 2003, **103**, 3155–3211; (d) M. Debnath, A. Dutta, S. Biswas, K. K. Das, H. M. Lee, J. Vicha, R. Marek, J. Marek and M. Ali, *Polyhedron*, 2013, **63**, 189–198.
- (a) M. R. Maurya, A. A. Khan, A. Azam, S. Ranjan, N. Mondal, A. Kumar, F. Avecilla and J. C. Pessoa, *Dalton Trans.*, 2010, **39**, 1345–1360; (b) L. Reytmán, O. Braitbard and E. Y. Tshuva, *Dalton Trans.*, 2012, **41**, 5241–5247; (c) O. Taheri, M. Behzad, A. Ghaffari, M. Kubicki, G. Dutkiewicz, A. Bezaatpour, H. Nazari, A. Khaleghian, A. Mohammadi and M. Salehi, *Transition Met. Chem.*, 2014, **39**, 253–259.
- (a) E. Kober, Z. Janas and J. Jezierska, *Inorg. Chem.*, 2016, **55**, 10888–10898; (b) P. Adão, J. C. Pessoa, R. T. Henriques, M. L. Kuznetsov, F. Avecilla, M. R. Maurya, U. Kumar and I. Correia, *Inorg. Chem.*, 2009, **48**, 3542–3561; (c) P. Adão, M. R. Maurya, U. Kumar, F. Avecilla, R. T. Henriques, M. L. Kuznetsov, J. C. Pessoa and I. Correia, *Pure Appl. Chem.*, 2009, **81**, 1279–1296; (d) I. Correia, J. C. Pessoa, M. T. Duarte, M. F. Minas da Piedade, T. Jakusch, T. Kiss, A. Dörnyei, M. M. C. A. Castro, C. F. G. C. Geraldés and F. Avecilla, *Eur. J. Inorg. Chem.*, 2005, 732–744; (e) I. Correia, J. C. Pessoa, M. T. Duarte, R. T. Henriques, M. F., M. da Piedade, L. F. Veiros, T. Jakusch, T. Kiss, A. Dörnyei, M. M. C. A. Castro, C. F. G. C. Geraldés and F. Avecilla, *Eur. J. Inorg. Chem.*, 2004, 2301–2317; (f) P. Adão, J. C. Pessoa, R. T. Henriques, M. L. Kuznetsov, F. Avecilla, M. R. Maurya, U. Kumar and I. Correia, *Inorg. Chem.*, 2009, **48**, 3542–3561.
- M. M. Hänninen, A. Peuronen, P. Damlin, V. Tyystjärvi, H. Kivelä and A. Lehtonen, *Dalton Trans.*, 2014, **43**, 14022–14028.
- (a) T. K. Paine, T. Weyhermüller, L. D. Slep, F. Neese, E. Bill, E. Bothe, K. Wieghardt and P. Chaudhuri, *Inorg. Chem.*, 2004, **43**, 7324–7338; (b) A. Jezierski and J. B. Raynor, *J. Chem. Soc., Dalton Trans.*, 1981, 1.
- T. Kajiwara, R. Wagner, E. Bill, T. Weyhermüller and P. Chaudhuri, *Dalton Trans.*, 2011, **40**, 12719–12726.
- S. R. Cooper, Y. B. Koh and K. N. Raymond, *J. Am. Chem. Soc.*, 1982, **104**, 5092–5102.
- P. R. Klich, A. T. Daniher, P. R. Challen, D. B. McConville and W. J. Youngs, *Inorg. Chem.*, 1996, **35**, 347–356.
- (a) Z. Liu and F. C. Anson, *Inorg. Chem.*, 2000, **39**, 274–280; (b) Z. Liu and F. C. Anson, *Inorg. Chem.*, 2001, **40**, 1329–1333; (c) E. Raamat, K. Kaupmees, G. Ovsjannikov, A. Trummal, A. Kütt, J. Saame, I. Koppel, I. Kaljurand, L. Lipping, T. Rodima, V. Pihl, I. A. Koppel and I. Leito, *J. Phys. Org. Chem.*, 2013, **26**, 162–170; (d) A. G. Cook and P. M. Feltman, *J. Chem. Educ.*, 2007, **84**, 1827–1829.
- (a) T. Sakumaroto, T. Moriuchi and K. Hirao, *J. Inorg. Biochem.*, 2016, **164**, 77–81; (b) T. Moriuchi, K. Ikeuchi and K. Hirao, *Dalton Trans.*, 2013, 11824–11830; (c) Z. Janas and P. Sobota, *Coord. Chem. Rev.*, 2005, **249**, 2144–2155; (d) R. A. Henderson, Z. Janas, L. B. Jerzykiewicz, R. L. Richards and P. Sobota, *Inorg. Chim. Acta*, 1999, **285**,

- 178–183; (e) S. C. Davies, D. L. Hughes, Z. Janas, L. Jerzykiewicz, R. L. Richards, J. R. Sanders and P. Sobota, *Chem. Commun.*, 1997, 1261–1262; (f) C. Le Floc'h, R. A. Henderson, P. B. Hitchcock, D. L. Hughes, Z. Janas, R. L. Richards, P. Sobota and S. Szafert, *J. Chem. Soc., Dalton Trans.*, 1996, 2755–2762.
- 13 T. A. Immel, U. Groth and T. Huhn, *Chem. – Eur. J.*, 2010, **16**, 2775–2789.
- 14 (a) P. Subramanian, J. T. Spence, R. Ortega and J. H. Enemark, *Inorg. Chem.*, 1984, **23**, 2564–2572; (b) C. J. G. Hinshaw, J. T. Peng, J. H. Spence, M. Enemark, L. Bruck, J. Kristofzski, S. L. Merbs, R. Ortega and P. A. Wexler, *Inorg. Chem.*, 1989, **28**, 4483–4491; (c) Y.-L. Wong, J.-F. Ma, W.-F. Law, Y. W.-T. Wong, Z.-Y. Zhang, T. C. W. Mak and D. K. P. Ng, *Eur. J. Inorg. Chem.*, 1999, 313–321; (d) E. Y. Tshuva, I. Goldberg and M. Kol, *J. Am. Chem. Soc.*, 2000, 10706–10707; (e) J. Balsells, P. J. Carroll and P. J. Walsh, *Inorg. Chem.*, 2001, **40**, 5568–5574; (f) S. Segal, I. Goldberg and M. Kol, *Organometallics*, 2005, **24**, 200–202; (g) J. England, C. R. Davies, M. Banaru and A. J. P. White, *Adv. Synth. Catal.*, 2008, **350**, 883–897; (h) T. A. Immel, U. Groth and T. Huhn, *Chem. – Eur. J.*, 2010, **16**, 2775–2789; (i) D. Peri, S. Meker, C. M. Manna and E. Y. Tshuva, *Inorg. Chem.*, 2011, **50**, 1030–1038; (j) T. Karimpur, E. Safaei, A. Wojtczak, Z. Jagličič and A. Kozakiewicz, *Inorg. Chim. Acta*, 2013, **395**, 124–134.
- 15 (a) C. Lorber, F. Wolff, R. Choukroun and L. Vendier, *Eur. J. Inorg. Chem.*, 2005, 2850–2859; (b) S. Groysman, S. Segal, M. Shamis, I. Goldberg, M. Kol, Z. Goldschmidt and E. Hayut-Salant, *J. Chem. Soc., Dalton Trans.*, 2002, 3425–3426; (c) A. W. Addison, T. N. Rao, J. Reedijk, J. Rijn and G. C. Verschoor, *J. Chem. Soc., Dalton Trans.*, 1984, 1349–1356.
- 16 (a) G. Hoshina, M. Tsuchimoto and S. Ohba, *Acta Crystallogr., Sect. C: Cryst. Struct. Commun.*, 1999, **55**, 1812–1813; (b) G. Hoshina, M. Tsuchimoto, S. Ohba, K. Nakajima, H. Uekusa, Y. Ohashi, H. Ishida and M. Kojima, *Inorg. Chem.*, 1998, **37**, 142–145; (c) C. R. Cornman, K. M. Geiser-Bush, S. P. Rowley and P. D. Boyle, *Inorg. Chem.*, 1997, **36**, 6401–6408.
- 17 (a) J. Krzystek, A. Ozarowski, J. Telser and D. C. Crans, *Coord. Chem. Rev.*, 2015, **301–302**, 123–133; (b) S. Ye, F. Neese, A. Ozarowski, D. Smirnov, J. Krzystek, J. Telser, J.-H. Liao, Ch.-H. Hung, W. Ch. Chu, Y.-F. Tsai, Ch. Wang, R.-Ch. Chen and H.-F. Hsu, *Inorg. Chem.*, 2010, **49**, 977–988.
- 18 A. Ozarowski and D. Reinen, *Inorg. Chem.*, 1986, **25**, 1704–1708.
- 19 B. Bleaney and K. D. Bowers, *Proc. R. Soc. London, Ser. A*, 1952, **214**, 451–465.
- 20 R. Maurice, K. Sivalingam, D. Ganyushin, N. Guihery, C. de Graaf and F. Neese, *Inorg. Chem.*, 2011, **50**, 6229–6236.
- 21 A. Ozarowski, C. J. Calzado, R. P. Sharma, S. Kumar, J. Jezierska, C. Angeli, F. Spizzo and V. Ferretti, *Inorg. Chem.*, 2015, **54**, 11916–11934.
- 22 J. Bendix, M. Brorson and C. E. Schaeffer, *Inorg. Chem.*, 1993, **32**, 2838–2849.
- 23 N. D. Chasteen, in *Biological Magnetic Resonance*, ed. L. J. Berliner and J. Reuben, Plenum, New York, 1981, vol. 3, pp. 53–119, Fig. 17.
- 24 (a) A. S. Ceccato, A. Neves, M. A. de Brito, S. M. Drechsel, A. S. Mangrich, R. Werner, W. Haase and A. J. Bortoluzzi, *J. Chem. Soc., Dalton Trans.*, 2000, 1573–1577; (b) M. Mikuriya and M. Fukuya, *Bull. Chem. Soc. Jpn.*, 1996, **69**, 679–683; (c) A. Neves, K. Wieghardt, B. Nuber and J. Weiss, *Inorg. Chim. Acta*, 1988, **150**, 183–187; (d) K. Wieghardt, U. Bossek, K. Volckmar, W. Swiridoff and J. Weiss, *Inorg. Chem.*, 1984, **23**, 1387–1389.
- 25 N. F. Chilton, R. P. Anderson, L. D. Turner, A. Soncini and K. S. Murray, *J. Comput. Chem.*, 2013, **34**, 1164–1175; L. Noodleman, Valence Bond Description of Antiferromagnetic Coupling in Transition Metal Dimers, *J. Chem. Phys.*, 1981, **74**(10), 5737–5743.
- 26 L. Noodleman and E. R. Davidson, *Chem. Phys.*, 1986, **109**(1), 131–143.
- 27 J. P. Malrieu, R. Caballol, C. J. Calzado, C. de Graaf and N. Guihery, *Chem. Rev.*, 2014, **114**, 429–492.
- 28 A. Rodríguez-Fortea, P. Alemany, S. Alvarez and E. Ruiz, *Inorg. Chem.*, 2002, **41**, 3769–3778.
- 29 A. Bencini and D. Gatteschi, *J. Am. Chem. Soc.*, 1980, **108**, 5763–5771.
- 30 F. Neese, *ORCA – An Ab Initio, Density Functional and Semiempirical Program Package, Version 4.0.1*, Surf Sara, Amsterdam, 2017; F. Neese, The ORCA Program System, *Wiley Interdiscip. Rev. Comput. Mol. Sci.*, 2012, **2**, 73–78.
- 31 A. Schäfer, H. Horn and R. Ahlrichs, *J. Chem. Phys.*, 1992, **97**(4), 2571–2577.
- 32 The Ahlrichs auxiliary basis sets (<https://www.basissetexchange.org/>) have been hardwired into the ORCA software.
- 33 K. Eichkorn, F. Weigend, O. Treutler and R. Ahlrichs, *Theor. Chem. Acta*, 1997, **97**(1–4), 119–124.
- 34 C. Duboc, D. Ganyushin, K. Sivalingam, M.-N. Collomb and F. Neese, *J. Phys. Chem. A*, 2010, **114**, 10750–10758.
- 35 A. Pascual-Alvarez, J. Vallejo, E. Pardo, M. Julve, F. Lloret, J. Krzystek, D. Armentano, W. Wernsdorfer and J. Cano, *Chem. – Eur. J.*, 2015, **21**, 17299–17307.
- 36 F. Weigend and R. Ahlrichs, *Phys. Chem. Chem. Phys.*, 2005, **18**, 3297–3305.
- 37 (a) C. Van Stappen, D. Maganas, S. DeBeer, E. Bill and F. Neese, *Inorg. Chem.*, 2018, **57**, 6421–6438; (b) J. Krzystek, A. T. Fiedler, J. J. Sokol, A. Ozarowski, S. A. Zvyagin, T. C. Brunold, J. R. Long, L. C. Brunel and J. Telser, *Inorg. Chem.*, 2004, **43**, 5645–5458.
- 38 C. J. Whiteoak, G. J. P. Britovsek, V. C. Gibson and A. J. White, *Dalton Trans.*, 2009, 2337–2344.
- 39 A. Hassan, L. Pardi, J. Krzystek, A. Sienkiewicz, P. Goy, M. Rohrer and L.-C. Brunel, *J. Magn. Reson.*, 2000, **142**(2), 300–312.
- 40 G. A. Bain and J. F. Berry, *J. Chem. Educ.*, 2008, **85**, 532–536.
- 41 *CrysAlis CCD and CrysAlis RED*, Oxford Diffraction, Wroclaw, Poland, 2009.
- 42 G. Sheldrick, *Acta Crystallogr., Sect. C: Struct. Chem.*, 2015, **71**, 3–8.